Phase diagram of a bilayer superconductor under an in-plane magnetic field

Uddalok Nag,[1] Jonathan Schirmer,[1,2] Enrico Rossi,[2] Chao-Xing Liu,[1] and J. K. Jain[1]
[1]*Department of Physics, 104 Davey Laboratory, The Pennsylvania State University, University Park, Pennsylvania 16802, USA*
[2]*Department of Physics, William and Mary, Williamsburg, Virginia 23187, USA*

(Received 6 August 2024; revised 9 September 2025; accepted 26 September 2025; published 16 October 2025)

We study a double layer superconductor in the presence of a parallel magnetic field B by obtaining self-consistent solutions of the Bogoliubov–de Gennes equations, and also using the Pokrovsky-Talapov model for the free energy expressed in terms of the relative phase, namely the difference in the phases of the superconducting order parameters in the two layers. We find that with increasing B a continuous transition occurs from the BCS state, where the relative phase is constant, into a state which contains stripes of the BCS state separated by localized vortices in the relative phase. This state is predicted to manifest through oscillations in the amplitude of the superconducting gap and an alternating pattern of supercurrents. With increasing B, the BCS stripe state continuously evolves into the Fulde-Ferrell-Larkin-Ovchinnikov state with linearly varying relative phase and a constant gap amplitude. These predictions apply to superconductivity in bilayer transition-metal-dichalcogenide systems with Ising spin-orbit coupling, and ought to be testable in a recently studied experimental system.

DOI: 10.1103/gnth-5ssq

I. INTRODUCTION

In a system with time reversal and spatial inversion symmetry, Cooper pairs with zero momentum are stabilized, as assumed in Bardeen-Cooper-Schrieffer (BCS) theory. But if either of these symmetries is broken, for example the time reversal symmetry (due to a magnetic field) or spatial inversion symmetry (due to antisymmetric spin-orbit coupling), the resulting Cooper pairs can have nonzero center of mass momentum $\boldsymbol{q}$, producing the Fulde-Ferrell-Larkin-Ovchinnikov (FFLO) superconducting state described by a gap parameter of the form $\Delta(\boldsymbol{r}) = |\Delta(\boldsymbol{r})|e^{i\boldsymbol{q}\cdot\boldsymbol{r}}$ [1–4]. Even though the FFLO state was predicted six decades ago, its realization has been challenging and it has been reported in very few condensed matter [5,6] and atomic systems [4,7,8].

Liu considered a bilayer Ising superconductor (SC) in the presence of a parallel magnetic field using the Ginzburg-Landau (GL) approach [9]. With increasing magnetic field, a phase transition was predicted from the BCS state into a state with the gap function $\Delta_{\pm}(x) = |\Delta|e^{\pm iqx}$, where $\pm$ labels two SC layers. As $|\Delta|$ is spatially uniform and each SC layer has a single q value, this state is an FFLO state, also called the "layer helical state." Indirect evidence for the phase transition predicted in Ref. [9] has been observed in bilayer or multilayer Ising SCs [10,11], characterized by an upturn in the in-plane upper critical magnetic field, accompanied by broken translational and rotational symmetries, when lowering temperatures [12].

Given the experimental feasibility of this remarkable physics, we theoretically evaluate the phase diagram of a bilayer SC in the presence of an in-plane B by obtaining self-consistent solutions of the Bogoliubov–de Gennes (BdG) equations for electrons on a lattice subject to an attractive Hubbard U interaction. The BdG formalism, which is valid for a wider range of parameters than the GL approach (valid only near the critical temperature) and also allows for spatial variation of the complex gap function, reveals striking physics beyond that in Ref. [9]. Most remarkably, as the magnetic field is increased, a transition takes place into a state that consists of stripes of the BCS state separated by interlayer vortices (namely 2π phase winding of the order parameter between two layers), as shown schematically in the inset of Fig. 1(a). This "BCS stripe" or vortex lattice state continuously evolves into a uniform FFLO state (or the layer helical state) of Ref. [9] as the magnetic field is further increased. An immediately testable prediction of our work is that the state occurring close to the transition line in the experiment of Ref. [11] is a a BCS stripe state, the striped character of which can be revealed by a measurement of the local order parameter, the amplitude of which should show periodic oscillations in the direction perpendicular to the magnetic field, as well as by the distribution of local supercurrent. This, we believe, will provide a more direct and definitive confirmation of the underlying FFLO physics in Ref. [11]. We show that an effective Pokrovsky-Talapov theory with Josephson coupling captures certain qualitative features described above.

II. MODEL HAMILTONIAN AND METHOD

We model each layer of the double-layer SC as a square lattice, with intralayer hopping $t_1 = 1$ and an interlayer hopping t [inset of Fig. 1(c)]. In this work, we report all our energies and temperature in units of t_1. Superconductivity is incorporated through an on-site attractive interaction term, i.e. a negative-U Hubbard model. The Hamiltonian is given by $\mathcal{H} = \mathcal{H}_0 + \mathcal{H}_I$ with

$$\begin{aligned}\mathcal{H}_0 = &-\sum_{\hat{\delta},l,\boldsymbol{j},\sigma}\left(e^{iA^l_{\hat{\delta},\boldsymbol{j}}}c^{\dagger}_{l,\boldsymbol{j}+\hat{\delta},\sigma}c_{l,\boldsymbol{j},\sigma} + e^{-iA^l_{\hat{\delta},\boldsymbol{j}}}c^{\dagger}_{l,\boldsymbol{j},\sigma}c_{l,\boldsymbol{j}+\hat{\delta},\sigma}\right)\\ &-t\sum_{\boldsymbol{j},\sigma}\left(e^{iA_{z,\boldsymbol{j}}}c^{\dagger}_{+,\boldsymbol{j},\sigma}c_{-,\boldsymbol{j},\sigma} + e^{-iA_{z,\boldsymbol{j}}}c^{\dagger}_{-,\boldsymbol{j},\sigma}c_{+,\boldsymbol{j},\sigma}\right)\\ &-\mu\sum_{\boldsymbol{j},l,\sigma}c^{\dagger}_{l,\boldsymbol{j},\sigma}c_{l,\boldsymbol{j},\sigma},\end{aligned} \tag{1}$$

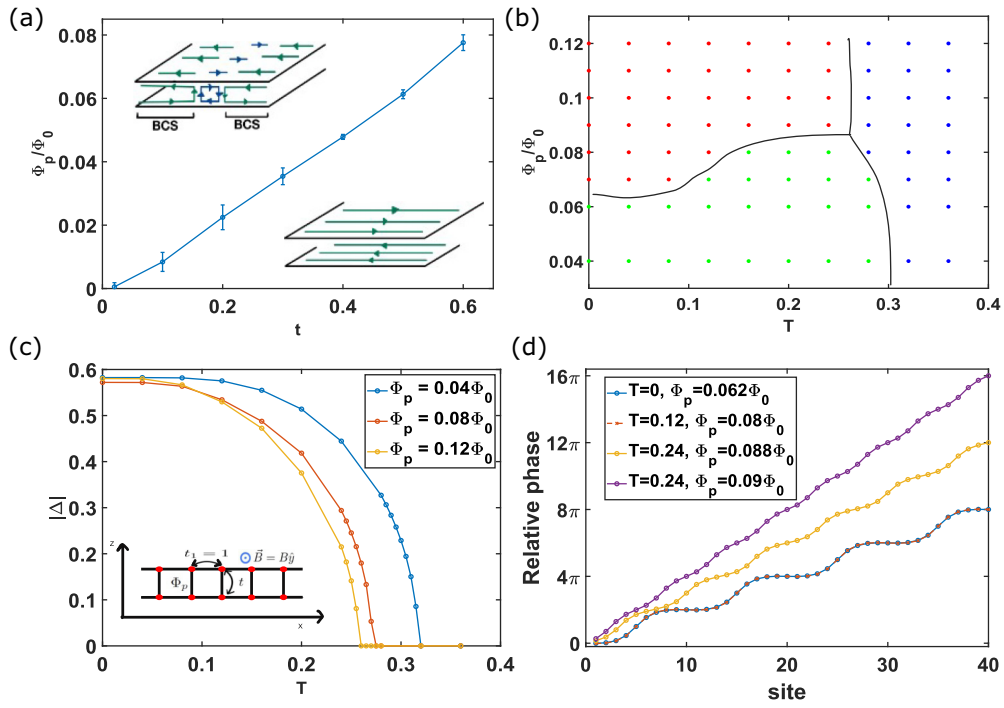

FIG. 1. (a) B-t phase diagram at $T = 0$, $U = 4$, and $\mu = -3$. The error in the thermodynamic value of the critical flux is determined by performing linear fits of the data in Fig. 4, with different numbers of points. The insets show schematics of the current flow patterns for the two states. (b) The B-T phase diagram for $U = 4$, $\mu = -3$, $N = 40$, and $t = 0.5$. The green, red, and blue dots show BCS, stripe, and normal states. (c) The average gap amplitude as a function of temperature for three different values of Φ_p/Φ_0 for $U = 4$, $\mu = -3$, $N = 40$, and $t = 0.5$. (d) The relative phase at four different points in panel (b) as we first move along the transition line from BCS to stripe state and then along the BCS to normal state. The plots for $T = 0$, $\Phi_p = 0.062\Phi_0$ and $T = 0.12$, $\Phi_p = 0.08\Phi_0$ coincide.

$$\mathcal{H}_{\mathcal{I}} = -U \sum_{\boldsymbol{j},l} c^{\dagger}_{l,\boldsymbol{j},\uparrow} c^{\dagger}_{l,\boldsymbol{j},\downarrow} c_{l,\boldsymbol{j},\downarrow} c_{l,\boldsymbol{j},\uparrow}. \tag{2}$$

The layers are taken to be parallel to the x-y plane, $l = \pm$ and $\sigma = \uparrow, \downarrow$ are the layer and spin indices, $\boldsymbol{j} \equiv (j_x, j_y)$ labels the lattice sites in a plane, and $\hat{\delta} = \hat{x}, \hat{y}$ denotes in-plane unit vectors. The operator $c_{l,\boldsymbol{j},\sigma}$ annihilates an electron with spin σ at site $\boldsymbol{j}$ in layer l. The magnetic field is taken as $\boldsymbol{B} = B\hat{y}$. It is incorporated through $A^l_{\delta,\boldsymbol{j}}$ and $A_{z,\boldsymbol{j}}$, which are the Peierls phases for intra- and interlayer hoppings, determined by the condition that the phases around each plaquette add to $2\pi\,\Phi_p/\Phi_0$, where Φ_p is the flux per plaquette and $\Phi_0 = h/e$ is the flux quantum. We will work with the gauge choice, $A^l_{\hat{x},\boldsymbol{j}} = l\pi \times \Phi_p/\Phi_0$, and $A^l_{\hat{y},\boldsymbol{j}} = 0 = A_{z,\boldsymbol{j}}$. Note that this gauge choice does not break the periodicity of the lattice, implying that the in-plane magnetic field does not break the translational symmetry; in other words, we do not need to define a magnetic unit cell (MUC) and the flux Φ_p can take arbitrary values. We discuss the consequences of working with an MUC in Appendix A.

Note that we have not included either a Zeeman term for coupling of the magnetic field to the spin or the spin-orbit coupling. The Zeeman term is negligible in bilayer Ising superconductors for which the spin is pinned to the out-of-plane directions. As shown in Appendix B, the Ising spin-orbit coupling essentially renormalizes a hopping matrix element. The model considered here thus applies to superconductivity in transition-metal-dichalcogenide (TMD) bilayers with Ising spin-orbit coupling.

The mean field BdG Hamiltonian H_{MF}, bilinear in electron operators, is obtained by replacing the $\mathcal{H}_{\mathcal{I}}$ term by

$$\mathcal{H}_{\mathcal{I}} \to -\sum_{l,\boldsymbol{j}} \left(\Delta_{l,\boldsymbol{j}} c^{\dagger}_{l,\boldsymbol{j},\uparrow} c^{\dagger}_{l,\boldsymbol{j},\downarrow} + \Delta^{\star}_{l,\boldsymbol{j}} c_{l,\boldsymbol{j},\downarrow} c_{l,\boldsymbol{j},\uparrow} - \frac{|\Delta_{l,\boldsymbol{j}}|^2}{U} \right), \tag{3}$$

$$\Delta_{l,\boldsymbol{j}} = U \langle c_{l,\boldsymbol{j},\downarrow} c_{l,\boldsymbol{j},\uparrow} \rangle, \tag{4}$$

where $\langle \cdots \rangle$ denotes the thermal average and $\Delta^{\star}_{l,\boldsymbol{j}}$ is the complex conjugate of $\Delta_{l,\boldsymbol{j}}$. We solve for this Hamiltonian for a square system of size $N \times N$ in the x-y plane. We take a unit cell of size 1 in the $\hat{y}$ direction, and let it span the entire system (N sites) in the $\hat{x}$ direction. So, counting two layers, we have $N \times 1 \times 2$ sites in the unit cell. We assume antiperiodic boundary conditions in both $\hat{x}$ and $\hat{y}$ directions to ensure Bloch states occur in both $\pm\boldsymbol{k}$. Note that these results should be valid even if we choose a different boundary condition, as discussed in Appendix C. We perform our calculation for various N values and extrapolate to $\frac{1}{N} \to 0$ to obtain the thermodynamic limits for various quantities. It is also useful to define the total flux through the system: $\Phi = N\Phi_p$.

To go to the momentum space, we write $\boldsymbol{j} = \boldsymbol{R}_j + \alpha\hat{x}$, where $\boldsymbol{R}_j = j_y\hat{y}$ is the position vector of the unit cell containing the site $\boldsymbol{j}$, and $\alpha = 1, \ldots, N$ is the in-plane site index within the unit cell. We then define the transformation: $c_{l,\boldsymbol{j},\sigma} = \frac{1}{N}\sum_{\boldsymbol{k}} e^{i\boldsymbol{k}\cdot\boldsymbol{R}_j} c_{l,\alpha,\sigma}(\boldsymbol{k})$, where $\boldsymbol{k} = \frac{\pi}{N} n_y \hat{y}$; $n_y = -(N-1), -(N-3), \ldots, (N-1)$ (n_y should only takes odd integer values, so we must choose N to be even). Defining an $8N$ dimensional vector

$\Psi(\boldsymbol{k}) = [\{c_{l,\alpha,\uparrow}(\boldsymbol{k})\}, \{c_{l,\alpha,\downarrow}(\boldsymbol{k})\}, \{c^\dagger_{l,\alpha,\uparrow}(-\boldsymbol{k})\}, \{c^\dagger_{l,\alpha,\downarrow}(-\boldsymbol{k})\}]^{\mathrm{T}}$, we obtain (closely following Ref. [13])

$$H_{\mathrm{MF}} = \frac{1}{2}\sum_{\boldsymbol{k}} \Psi^\dagger(\boldsymbol{k})\hat{\mathcal{H}}_{\mathrm{BdG}}(\boldsymbol{k})\Psi(\boldsymbol{k}) + \frac{1}{2}\sum_{\boldsymbol{k}} \mathrm{Tr}[H_0(\boldsymbol{k})] + \sum_{j,l}\frac{|\Delta_{l,j}|^2}{U}, \tag{5}$$

where $\hat{\mathcal{H}}_{\mathrm{BdG}}$ is an $8N \times 8N$ BdG matrix and $H_0(\boldsymbol{k})$ is the single particle part of the Hamiltonian in Fourier space. The eigenenergy spectrum of H_{MF} can be obtained by the diagonalization of $\hat{\mathcal{H}}_{\mathrm{BdG}}$.

To obtain self-consistent solutions we (i) begin with an initial guess $\Delta^{\mathrm{guess}}_{l,\alpha} = |\Delta| e^{\frac{il n\pi\alpha}{N}}$ on the site $\alpha = 1, \ldots, N$, which corresponds to n vortices in the entire system; (ii) construct the BdG Hamiltonian to calculate $\Delta_{l,\alpha}$ using Eq. (4); (iii) use this as our new guess; and (iv) repeat this process until we get a self-consistent result, defined by the condition that the relative difference between the absolute values of the gaps in two successive steps is less than some tolerance (typically taken to be 10^{-5}) at each site. We perform this for all values of $0 \leqslant n \leqslant \mathrm{Int}[2\Phi/\Phi_0] + 1$ and take the self-consistent solution with the lowest free energy $\mathcal{F} = \langle H_{\mathrm{MF}} - TS\rangle$, where the thermal average of the first term on the right hand side of Eq. (5) is given by $\frac{1}{2}\sum_{\boldsymbol{k},\beta} E_\beta(\boldsymbol{k}) n_F[E_\beta(\boldsymbol{k})]$ with $n_F(E) = (e^{E/(k_BT)} + 1)^{-1}$, and $\langle S\rangle = -k_B \sum_{k,\beta} (n_F[E_\beta(\boldsymbol{k})] \log n_F[E_\beta(\boldsymbol{k})] + \{1 - n_F[E_\beta(\boldsymbol{k})]\} \log\{1 - n_F[E_\beta(\boldsymbol{k})]\})$. We have tested the stability of the lowest-energy solution by adding a random variation to the initial guess. We discuss this in more detail in Appendix D. Our solutions have zero net current, as required by Bloch's theorem [14]. In Appendix E we argue that even though we are working with a lattice, our analysis should be valid in the continuum limit.

The in-plane current and that between two layers are given by $J_{\delta,l}(\boldsymbol{r_j}) = -\frac{\partial \mathcal{H}}{\partial A_{\delta,l}}$ and $J_z(\boldsymbol{r_j}) = -\frac{\partial \mathcal{H}}{\partial A_z}$, respectively [13]. The average current densities in the $\hat{x}$ and $\hat{z}$ directions are

$$\langle J^l_{x,\boldsymbol{j}}\rangle = i\sum_\sigma \left(e^{iA^l_{\hat{x},j}}\langle c^\dagger_{l,\boldsymbol{j}+\hat{x},\sigma} c_{l,\boldsymbol{j},\sigma}\rangle - e^{-iA^l_{\hat{x},j}}\langle c^\dagger_{l,\boldsymbol{j},\sigma} c_{l,\boldsymbol{j}+\hat{x},\sigma}\rangle\right),$$

$$\langle J_{z,\boldsymbol{j}}\rangle = it\sum_\sigma \left(e^{iA_{z,j}}\langle c^\dagger_{+,\boldsymbol{j},\sigma} c_{-,\boldsymbol{j},\sigma}\rangle - e^{-iA_{z,j}}\langle c^\dagger_{-,\boldsymbol{j},\sigma} c_{+,\boldsymbol{j},\sigma}\rangle\right)$$

and the average current density in the $\hat{y}$ direction vanishes. Note that even though H_{MF} breaks the $U(1)$ symmetry, the current density satisfies the continuity equation $\langle \nabla \cdot \boldsymbol{J}\rangle = 0$. This follows because the source term in the mean field equation that breaks the $U(1)$ symmetry identically vanishes when the self-consistency condition is imposed [15].

III. PHASE DIAGRAM

We first consider the $T = 0$ phase diagram and obtain for a given N the lowest-energy state to determine the critical values of Φ/Φ_0 below which the BCS state survives. We obtain the thermodynamic limit by extrapolation. (The number of vortices in the ground state varies as a function of N.) The resulting phase diagram is shown in Fig. 1(a) as a function of B and t.

To bring out the nature of the ground state, an important quantity is the relative phase, namely the gauge invariant difference between phases of the order parameter at two sites that lie directly across one another (i.e. have the same x-y coordinates) in the two layers. The Hamiltonian is invariant under the gauge transformation: $c_{l,j,\sigma} \to \tilde{c}_{l,j,\sigma} = e^{i\psi_{j,l}} c_{l,j,\sigma}$, $\Delta_{j,l} \to \tilde{\Delta}_{j,l} = e^{2i\psi_{j,l}}\Delta_{j,l}$, $A^l_{\hat{\delta},\boldsymbol{j}} \to \tilde{A}^l_{\hat{\delta},\boldsymbol{j}} = A^l_{\hat{\delta},\boldsymbol{j}} - \psi_{\boldsymbol{j}+\hat{\delta},l} + \psi_{\boldsymbol{j},l}$, and $A_{z,j} \to \tilde{A}_{z,\boldsymbol{j}} = A_{z,j} - \psi_{\boldsymbol{j},+} + \psi_{\boldsymbol{j},-}$ (the last two are needed to ensure the invariance of the hopping term). The gauge invariant relative phase is defined as $\arg(\Delta_{+,\alpha}/\Delta_{-,\alpha}) - 2A_{z,\alpha}$ with $A_{z,\alpha} = 0$ for our chosen gauge.

For sufficiently small Φ, the ground state is in the "BCS state." Here the relative phase is uniformly zero (the phases in the two layers are locked by interlayer tunneling and the gap can be taken to be real), the gap amplitude is constant, there are no interlayer supercurrents, and there are no spontaneous net currents, although the top and the bottom layers have equal and opposite diamagnetic currents [16].

The BCS state survives up to a critical magnetic flux. Figure 2(a) depicts the relative phase for a magnetic flux just above the critical value. Evidently, there are regions where the relative phase remains nearly constant separated by regions where it rapidly changes by 2π. Thus, rather than a relative phase linearly varying with x, the system finds it energetically favorable to create BCS stripes running parallel to the direction of the magnetic field. Associated with the formation of stripes is a periodic variation in the amplitude of the gap [Fig. 2(c)], and also the phase of the gap [Fig. 2(e)]. The stripe state also has a complex current pattern. Figure 2(g) displays the current in the top layer (J^+_x); the current in the bottom layer is $J^-_x = -J^+_x$ and the interlayer current can be deduced from the current at each lattice site. In the limit of large flux, we find the relative phase changes linearly with x, recovering the layer helical state of Ref. [9], with a net change of about $4\pi\Phi/\Phi_0$ across the system corresponding to two vortices per flux quantum, and the gap amplitude is nearly constant.

Intuitively, the BCS stripe state can be viewed as arising from a competition between the interlayer tunneling and the in-plane magnetic flux. While the interlayer tunneling tends to lock the SC order parameter phases between two layers, thus favoring the BCS state, the in-plane magnetic flux tends to drive a variation of this relative phase by introducing interlayer vortices to form the layer helical state. The highly nonuniform BCS stripe state emerges as a compromise between these two competing tendencies.

We have also evaluated the finite temperature phase diagram, shown in Fig. 1(b) for $t = 0.5$. Figure 1(c) shows how the gap amplitude varies as a function of T, where the gap $|\Delta|$ in the stripe state denotes the spatial average of the gap amplitude. The transitions from either the BCS or the stripe state to the normal state follow the standard behavior. The average gap amplitude varies smoothly across the transition from the BCS to the stripe state because the number of vortices per flux quantum rises continuously from zero. Figure 1(d) shows the behavior of the relative phase near the phase boundary separating the BCS and the stripe states as a function of T; the phase becomes more linear as T approaches T_c, consistent with Ref. [9].

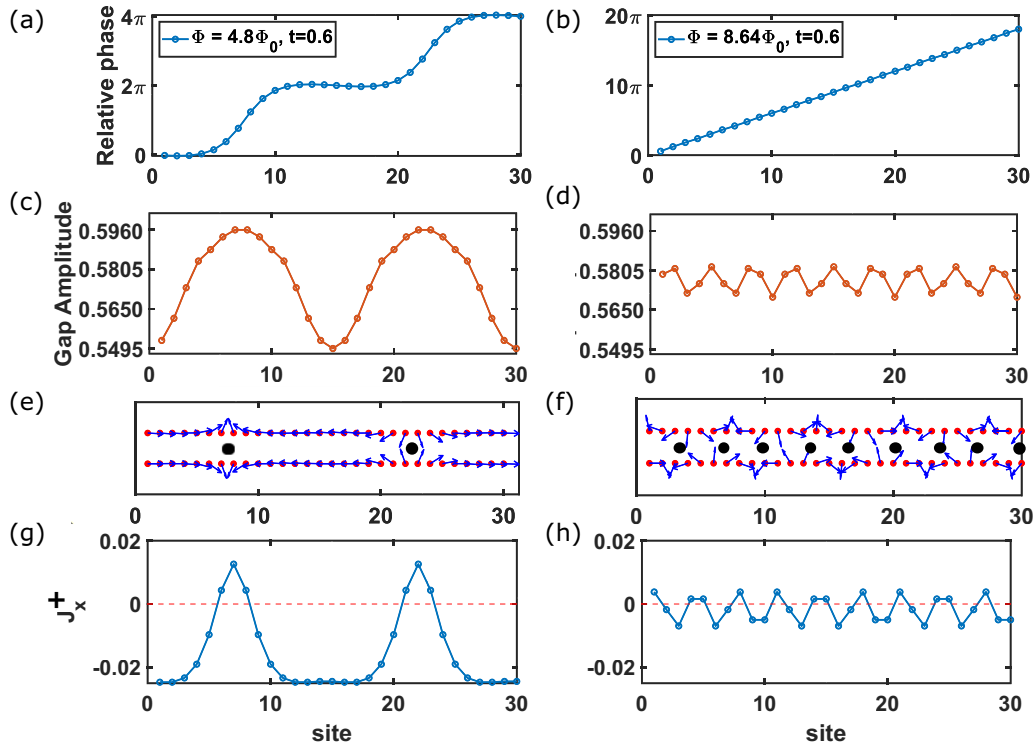

FIG. 2. BCS stripe state for a system of length $N = 60$ for different values of the magnetic field. (For clarity, we show only half of the system; this behavior repeats in the other half.) For small Φ/Φ_0 the state (not shown) has zero relative phase, spatially uniform gap, equal and opposite currents in two layers, and no interlayer current. The first column corresponds to a magnetic flux Φ just above the critical value, and the second corresponds to a high Φ. Spatial variations are shown for (a), (b) the relative phase (difference between the phases in two layers); (c), (d) the gap amplitude; (e), (f) the phase of Δ, shown by an arrow at each site, determined up to a global U(1) rotation; and (g), (h) the current density J_x^+ in the top layer. The magnitudes of the gap are the same in both layers. The current in the bottom layer is $J_x^- = -J_x^+$, from which the interlayer current may be deduced. The black dots in panels (e) and (f) show the positions of interlayer vortices in the gap parameter (determined up to a global translation). The parameters chosen are $U = 4, \mu = -3, T = 0, t = 0.6$. Note that for a large Φ the relative phase varies linearly with the position and the gap amplitude becomes nearly constant.

IV. EFFECTIVE MODEL

We now show that the qualitative features of the phase diagram can be captured by an effective theory. The free energy per unit length along the y direction takes a frustrated sine-Gordon form:

$$\mathcal{F}_{\text{eff}} = \rho_s \int dx \left[\frac{1}{2}(\partial_x \varphi - 2Bz_0)^2 - g\cos(\varphi) \right] \tag{6}$$

where φ is the relative phase between two layers, ρ_s is the phase stiffness, and the last term represents the Josephson coupling between the layers. This model is equivalent to the Pokrovsky-Talapov model used to study commensurate-incommensurate phase transitions [16–19]. We have neglected the fluctuations of the magnitude of the order parameter and assumed that φ is slowly varying in space. Details of the analysis of this model and its derivation from the microscopic Hamiltonian will be presented in a future work. In what follows, we outline some salient results.

The magnetic field B tends to wind φ, and in the absence of the Josephson coupling between layers ($g = 0$) φ varies linearly with position, yielding the FFLO state. On the other hand, the Josephson coupling tends to lock the relative phase at $\varphi = 2\pi n$ where $n \in \mathbb{Z}$, which is the BCS state. In general, these two effects compete, leading to the vortex lattice/stripe state. In particular, (6) admits two classes of solutions, depending on whether $\frac{1}{2\pi}\int dx \partial_x \varphi = N_v$ is zero or nonzero where N_v is the number of vortices in the system. If $N_v = 0$ then the minimum of (6) is $\varphi = 2\pi n$ (the BCS state) and the free energy per unit length in the x direction is $f_{\text{eff}} = -\rho_s(g - 2B^2 z_0^2)$. At a critical magnetic field $B_c = \frac{\sqrt{g}}{\pi^2 z_0}$, the state with a single vortex ($N_v = 1$) has the same energy as the BCS state, and higher magnetic fields yield the vortex lattice state, which we discuss below.

The saddle point equation of (6) is the one-dimensional sine-Gordon equation:

$$\partial_x^2 \varphi = g\sin(\varphi). \tag{7}$$

A family of exact solutions to (7) that describes the vortex lattice state may be expressed in terms of the Jacobi amplitude function $\text{am}(u, k)$:

$$\varphi_\epsilon(x) = 2\,\text{am}\left(\sqrt{\epsilon}\,x, \frac{g}{\epsilon}\right) + \pi \tag{8}$$

where the solutions are labeled by the parameter $\epsilon \geqslant g$, and for each solution ϵ is given by the value of the "integral of

motion":

$$\epsilon = \frac{1}{4}(\partial_x \varphi_\epsilon)^2 + \frac{g}{2}[\cos(\varphi_\epsilon) + 1]. \tag{9}$$

Plugging (8) into (6), we may express the free energy per unit length in the x direction as

$$f_{\text{eff}}(\chi, \omega) = \rho_s g\left[-\frac{1}{\chi^2} + \frac{2E(\chi^2)}{\chi^2 K(\chi^2)} - \frac{\pi\omega}{\chi K(\chi^2)}\right] \tag{10}$$

where $\chi = \sqrt{g/\epsilon}$ and $\omega = Bz_0/\sqrt{g}$. We have neglected the magnetic energy $2\rho_s B^2 z_0^2$ since it is just a constant shift. K is the elliptic integral of the first kind and E is the complete elliptic integral. For a fixed value of ω, f_{eff} should be minimized with respect to χ:

$$\frac{1}{\rho_s g}\frac{\partial f_{\text{eff}}}{\partial \chi} = 4(\chi^2 - 1)K^2(\chi^2) - E(\chi^2)[2E(\chi^2) - \pi\omega\chi] = 0. \tag{11}$$

By the implicit function theorem, the solution $\chi(\omega)$ is a differentiable function of ω. Therefore, the solutions (8) evolve continuously as a function of B, and no phase transition is encountered for $B > B_c$, consistent with our BdG study above. In particular, for $\epsilon = g$, the solution is a single vortex:

$$\varphi_\epsilon(x) = 2\text{am}\left(\sqrt{g}x, 1\right) + \pi = 4\arctan(e^{\sqrt{g}x}), \tag{12}$$

and for $\epsilon \gg g$ the solution

$$\varphi_\epsilon(x) = 2\text{am}\left(\sqrt{\epsilon}x, 0\right) + \pi = 2\sqrt{\epsilon}x + \pi \tag{13}$$

describes the FFLO state.

V. DISCUSSION

The interplay between superconductivity and magnetic field in two-dimensional systems has been of interest in numerous contexts, including the possibility of topological superconductivity supporting Majorana zero modes [20–33]. Here we predict a stripe state in a bilayer superconductor exposed to a parallel magnetic field.

An earlier Landau-Ginzburg treatment of this problem by Liu [9] assumes the layer helical state ansatz $\Delta_l(\boldsymbol{r}) = |\Delta| e^{ilqx}$ where $l = \pm$ is the layer index and q is spatially uniform. He finds $q_c = \frac{2eBz_0}{2\hbar}$ in the limit of large B, where z_0 is the distance between two layers; the relative phase difference $2q_c x$ changes by 2π in a distance $\Delta x = 2\pi/2q_c$, which contains $Bz_0\Delta x = \Phi_0/2$ flux quanta, thus producing twice as many vortices as the number of flux quanta. In contrast, the highly nonuniform stripe state found in this work cannot be represented by a layer helical state with a single q in each layer. Qiu and Zhou [16] have also studied this problem within the Landau-Ginzburg formalism, while assuming that the gap function has the periodicity of an MUC containing one flux quantum (the ratio of the number of vortices to the number of flux quanta can take only discrete values in this model); this periodicity results in a Bloch wave solution for the superconducting order parameter and a commensurate-incommensurate phase transition. The BCS stripe state in our work does not respect the periodicity of the MUC, and thus does not belong to the Bloch wave solution.

By obtaining the self-consistent solutions of the BdG equations, we have shown that the application of a parallel B causes a transition into a stripe state. We thus predict that the phase transition observed in 2H-stacked $NbSe_2$ in Ref. [11] is into a stripe state with spatially varying gap amplitude, which adiabatically evolves into the uniform-gap layer-helical/FFLO state of Ref. [9] for large B. This stripe state may be identified most directly by measuring the oscillations in the amplitude of the gap, which are predicted to be strongest at low temperatures near the phase boundary.

We finally note that the BdG formalism employed in our calculation neglects the physics arising from the fluctuations in the phase of the gap, which will be important close to T_c. In principle, the transition from the superconducting to the normal state will be a Berezinskii-Kosterlitz-Thouless type. However, our model ought to be valid for $T << T_c$.

ACKNOWLEDGMENTS

U.N., J.S. (at The Pennsylvania State University), and J.K.J. were supported in part by the U.S. Department of Energy (DOE), Office of Basic Energy Sciences (BES), under Grant No. DE-SC0005042. Work by J.S. and E.R. was supported by the DOE, Office of Science, BES under Grant No. DE-SC0022245. C.-X.L acknowledges support from the NSF through The Pennsylvania State University Materials Research Science and Engineering Center (Grant No. DMR-2011839). We acknowledge Advanced CyberInfrastructure computational resources provided by The Institute for CyberScience at The Pennsylvania State University.

DATA AVAILABILITY

The datasets generated and analyzed during this study are openly available in the GitHub repository [34] under the Creative Commons Zero v1.0 Universal (CC0 1.0) license.

APPENDIX A: CONSEQUENCES OF CHOOSING A MAGNETIC UNIT CELL

As we mentioned in the main text, we have not chosen an MUC. This is because the in-plane magnetic field does not break the translation symmetry, as is evident from our choice of gauge. We show here that the results change qualitatively and quantitatively when we do choose a magnetic unit cell, because by choosing the SC gap to have the same periodicity as an MUC, we are restricting the allowed space of solutions. For illustration, we will choose a magnetic unit cell with one flux quantum passing through, as in Ref. [16].

We choose the size of the MUC to be of length $M = m$ in the $\hat{x}$ direction, where m is an integer and the flux per plaquette is $\Phi_p = \Phi_0/m$. So the dimensions of the MUC are $M \times 1 \times 2$ in the xyz coordinates. We choose $\Delta_{l,j}$ to have the same periodicity as the MUC. For our calculations, we choose $L \times ML$ MUCs in the $\hat{x}$ and $\hat{y}$ direction respectively, so the full system is a square of size ML, with $L = 12$. We assume antiperiodic boundary conditions to ensure Bloch states occur in both $\pm\boldsymbol{k}$. To go to the momentum space, we define $\boldsymbol{j} = \boldsymbol{R_j} + \alpha\hat{x}$, where $\boldsymbol{R_j} = [\frac{j_x}{M}]M\hat{x} + j_y\hat{y}$ (we have used the notation $[x]$ to denote the integer part of x) is the position vector of the MUC containing $\boldsymbol{j}$, and $\alpha = 1, \ldots, M$ is the in-plane site index within the MUC.

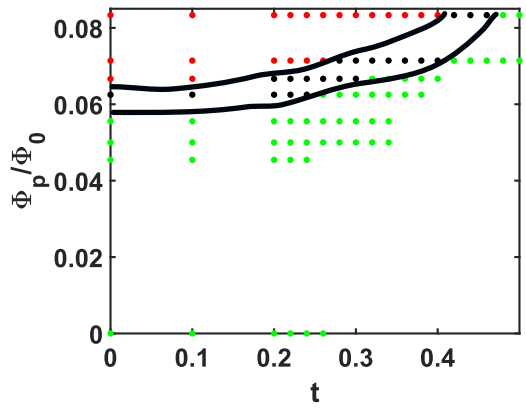

FIG. 3. The B-t phase diagram computed at $T = 0$, $U = 4$, and $\mu = -3$ obtained using a model in which we have chosen an MUC corresponding to one flux quantum. The green, black, and red points show states with no vortices (called the BCS state), a state with one vortex per flux quantum, and a state with two vortices per flux quantum, respectively

We then proceed similarly as in the main text, defining the Fourier transformed creation and annihilation operators with the allowed momentum values to be $\boldsymbol{k} = \frac{\pi}{ML}(n_x\hat{x} + n_y\hat{y})$; $n_x = -(M-1), -(M-3), \ldots, (M-1)$; and $n_y = -(ML-1), -(ML-3), \ldots, (ML-1)$. Both n_x and n_y can only take odd values, so we must choose M (and m) to be even. Following the procedure in the main text, we arrive at an expression that looks exactly the same as Eq. (5), but with the newly defined momentum values and an $8M \times 8M$ matrix for $\mathcal{H}_{\mathrm{BdG}}$.

The phase diagram computed using this method is shown in Fig. 3. Comparing with Fig. 1, we can see that there are both qualitative and quantitative differences.

(i) In Fig. 3, a much higher value of magnetic field is needed for vortices to go in. This is because we are missing solutions with vortices which do not have the same periodicity as the MUC.

(ii) In Fig. 3 there are discreet stripe states. This is because the imposed boundary condition allows only an integer number of vortices to pass through one MUC.

We note differences from the phase diagram calculated in Ref. [16]. The phase diagram we calculated in Fig. 3 is calculated at zero temperature, while the authors in Ref. [16] use a Ginzburg-Landau approach, which is only valid near the critical temperature.

APPENDIX B: MAPPING THE BILAYER TMD SYSTEM WITH ISING SPIN-ORBIT COUPLING TO OUR MODEL

In this Appendix, we demonstrate that the model we used can serve as the low-energy theory of the bilayer TMD system with Ising spin-orbit coupling. We start from the continuous model for a TMD monolayer. The single particle Hamiltonian for the layer l ($l = \pm$) at zero magnetic field reads

$$\mathcal{H}_{0,l}(\boldsymbol{p} = \epsilon\boldsymbol{K} + \boldsymbol{k}) = \xi_k + l\epsilon\beta_{\mathrm{SOC}}s_z, \tag{B1}$$

where ξ_k is the kinetic energy term, $\epsilon = \pm$ is the valley index, β_{SOC} is the Ising spin-orbit coupling strength, and s_z is the Pauli matrix for the spin degree of freedom. In the second quantization notation with the electron annihilation operator denoted as $c_{\boldsymbol{k},\epsilon,l,s}$ (s being the spin index), the Hamiltonian takes the form

$$\hat{H}_0 = \sum_{\boldsymbol{k},\epsilon,s,s'} c^\dagger_{\boldsymbol{k},\epsilon,l,s}[\mathcal{H}_{0,l}(\epsilon\boldsymbol{K} + \boldsymbol{k})]_{s,s'}c_{\boldsymbol{k},\epsilon,l,s'}. \tag{B2}$$

One can see that this Hamiltonian has a diagonal form with the spin-valley-layer locking, namely $\langle\epsilon = +, \uparrow|\hat{H}_{0,l}|\epsilon = +, \uparrow\rangle = \xi_k + l\beta_{\mathrm{SOC}}$, $\langle\epsilon = +, \downarrow|\hat{H}_{0,l}|\epsilon = +, \downarrow\rangle = \xi_k - l\beta_{\mathrm{SOC}}$, $\langle\epsilon = -, \uparrow|\hat{H}_{0,l}|\epsilon = -, \uparrow\rangle = \xi_k - l\beta_{\mathrm{SOC}}$, and $\langle\epsilon = -, \downarrow|\hat{H}_{0,l}|\epsilon = -, \downarrow\rangle = \xi_k + l\beta_{\mathrm{SOC}}$ for nonzero Hamiltonian matrix elements. Since we only wish to consider the lowest-energy bands and assume $\beta_{\mathrm{SOC}} > 0$, we project the full Hamiltonian onto the basis $A = \{|l = -, \epsilon = +, \uparrow\rangle, |l = -, \epsilon = -, \downarrow\rangle, |l = +, \epsilon = +, \downarrow\rangle, |l = +, \epsilon = -, \uparrow\rangle\}$. The low-energy Hamiltonian then becomes

$$\hat{H}_0^{\mathrm{low}} = \sum_{\boldsymbol{k},\alpha\in A}(\xi_k - \beta_{\mathrm{SOC}})c^\dagger_{\boldsymbol{k},\alpha}c_{\boldsymbol{k},\alpha}.$$

Note that the spin-valley indices are opposite for the two layers in the above basis wave functions, and this will have substantial influence on the interlayer tunneling.

The interlayer tunneling term in the original basis (before projecting onto the lowest-energy bands) preserves both spin and valley:

$$\hat{H}_t = -t\sum_{\boldsymbol{k},\epsilon,s}(c^\dagger_{\boldsymbol{k},\epsilon,-,s}c_{\boldsymbol{k},\epsilon,+,s} + c^\dagger_{\boldsymbol{k},\epsilon,+,s}c_{\boldsymbol{k},\epsilon,-,s}).$$

But, for $l = -$ and $+$, the spin and valley indices are opposite for low-energy bands in the basis set A. Therefore the direct tunneling from this term in the low-energy theory is zero. Interlayer tunneling between low-energy bands can, however, be mediated by the combination of $\hat{H}_t$ and the Zeeman coupling from the in-plane magnetic field.

We consider the in-plane magnetic field along the $\hat{x}$ direction. The Zeeman coupling is then given by

$$\hat{H}_Z = gB_x\sum_{\boldsymbol{k},l,\epsilon,s} c^\dagger_{\boldsymbol{k},\epsilon,l,s}(\sigma_x)_{s,s'}c_{\boldsymbol{k},\epsilon,l,s'},$$

where g is the g factor. From the Hamiltonian forms of $\hat{H}_t$ and $\hat{H}_Z$, we see that while the interlayer tunneling term pre-

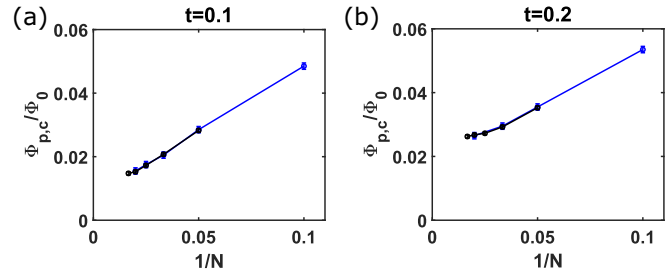

FIG. 4. Determination of the thermodynamic limit ($N \to \infty$) for the critical flux per plaquette, $\Phi_{p,c}$, for (a) $t = 0.1$ and (b) $t = 0.2$. We have chosen $U = 4$ and $\mu = -3$. The data points in blue correspond to the critical flux calculated assuming a periodic boundary condition, and the data points in black correspond to an antiperiodic boundary condition. We extrapolate both to the limit $1/N \to 0$ using a linear fit to get the values in Fig. 1(a).

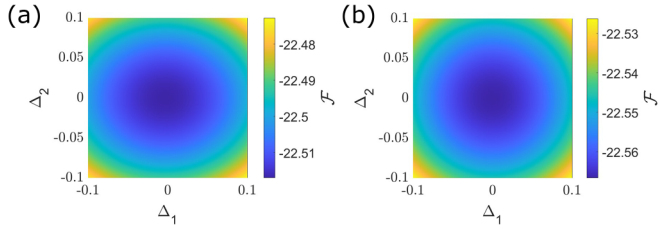

FIG. 5. Free energy ($\mathcal{F}$) profile around the ground state for (a) $U = 4$, $\mu = -3$, $t = 0.5$, $\Phi_p = 0.06\Phi_0$, $N = 40$, $T = 0$ and (b) $U = 4$, $\mu = -3$, $t = 0.5$, $\Phi_p = 0.12\Phi_0$, $N = 40$, $T = 0$ as a function of Δ_1 and Δ_2.

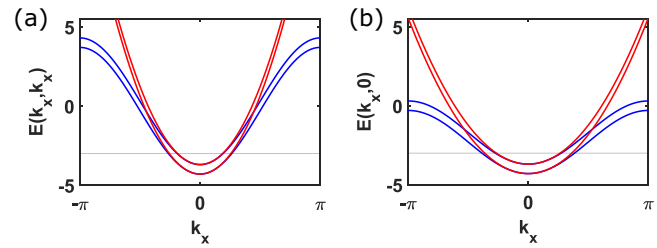

FIG. 6. (a) The band structure along $k_y = 0$. (b) The band structure along $k_x = k_y$. The blue lines are the energy dispersion for our lattice system; red lines are parabolas fit near the origin. (There are two bands because of two layers.) The plots are for $U = 4$, $t = 0.3$, $\mu = -3$, and zero magnetic field. The thin horizontal line marks the Fermi energy.

serves the spin-valley index while changing the layer index, the Zeeman term for an in-plane magnetic field changes the spin index while preserving the other two. Thus, we get an effective tunneling between the lowest-energy bands from the second order term in perturbation theory:

$$\hat{H}_t^{\text{low}} = \frac{tgB_x}{\beta_{\text{SOC}}} \sum_{\boldsymbol{k}} [c^\dagger_{\boldsymbol{k},+,-,\uparrow} c_{\boldsymbol{k},+,+,\downarrow} + c^\dagger_{\boldsymbol{k},-,-,\downarrow} c_{\boldsymbol{k},-,+,\uparrow} + \text{H.c.}].$$

The effective low-energy theory is given by

$$\hat{H}^{\text{low}} = \hat{H}_0^{\text{low}} + \hat{H}_t^{\text{low}}.$$

Due to the redundancy in the labeling of the basis wave functions, we can remove the valley index in the notation, so that $|l = -, \epsilon = +, \uparrow\rangle \to |l = -, \uparrow\rangle$, $|l = -, \epsilon = -, \downarrow\rangle \to |l = -, \downarrow\rangle$, $|l = +, \epsilon = +, \downarrow\rangle \to |l = +, \uparrow\rangle$, $|l = +, \epsilon = -, \uparrow\rangle \to |l = +, \downarrow\rangle$, and $\frac{tgB_x}{\beta_{\text{SOC}}} \to t$. The resulting Hamiltonian is a model for the spinful electrons in a bilayer system. We may include the orbital effect of the magnetic field by performing the Peierls substitution and then implement the lattice regularization for $\hat{H}^{\text{low}}$ to transform it to the lattice model, and with that, we can recover the noninteracting Hamiltonian $\mathcal{H}_0$ in the main text. Thus, the in-plane Zeeman effect only provides a correction to the interlayer tunneling parameter t.

APPENDIX C: PERIODIC VS ANTIPERIODIC BOUNDARY CONDITIONS

While we assume an antiperiodic boundary condition for all our calculations, in Fig. 4, we have compared the results for the critical flux density $\Phi_{p,c}$ (defined as the minimum flux density above which the system allows vortices to enter) assuming both periodic and antiperiodic boundary conditions. As we can see, the results for the critical flux density coincide for both periodic and antiperiodic boundary conditions.

APPENDIX D: STABILITY OF SOLUTIONS

We take multiple initial guesses and identify the solution with the lowest energy (which in general is given by most of the initial guesses). We add a small random perturbation to this solution as another guess, and always find that the self-consistent algorithm takes us back to the original lowest-energy solution, which ensures that it is not a local minimum. In Fig. 5, we have have taken two solutions and added a perturbation $\Delta_1 + i\Delta_2$ at each site, and calculated the free energy ($\mathcal{F} = \langle H_{\text{MF}} - TS \rangle$) as a function of Δ_1 and Δ_2, to verify we are indeed at a minimum. (Note that here we are only varying two parameters, but there are $4N$ possible independent parameters, two corresponding to each site in the unit cell.) Finally, the continuity of our phase diagram as we vary parameters of the Hamiltonian gives us full confidence that we have succeeded in finding the minimum energy solution.

APPENDIX E: CONTINUUM LIMIT

In our calculation, the lattice model allows us to obtain self-consistent results (because the number of parameters we need to obtain self-consistently is finite). However we believe our results should also be valid in the continuum limit. To ensure this, we have chosen $\mu = -3$ in our calculations, to ensure the Fermi surface is quite close to the bottom of the band (which extends from $-4 - t$ to $4 + t$ in units of interlayer coupling). As shown in Fig. 6, this lies in the region where the energy dispersion is nearly parabolic.

[1] P. Fulde and R. A. Ferrell, Superconductivity in a strong spin-exchange field, Phys. Rev. **135**, A550 (1964).
[2] A. I. Larkin and Y. N. Ovchinnikov, Nonuniform state of superconductors, Sov. Phys. JETP **20**, 762 (1965).
[3] D. F. Agterberg, Magnetoelectric effects, helical phases, and FFLO phases, in *Non-Centrosymmetric Superconductors: Introduction and Overview* (Springer, New York, 2012), pp. 155–170.
[4] J. J. Kinnunen, J. E. Baarsma, J.-P. Martikainen, and P. Törmä, The Fulde-Ferrell-Larkin-Ovchinnikov state for ultracold fermions in lattice and harmonic potentials: A review, Rep. Prog. Phys. **81**, 046401 (2018).
[5] A. Bianchi, R. Movshovich, C. Capan, P. G. Pagliuso, and J. L. Sarrao, Possible Fulde-Ferrell-Larkin-Ovchinnikov superconducting state in $CeCoIn_5$, Phys. Rev. Lett. **91**, 187004 (2003).

[6] Y. Matsuda and H. Shimahara, Fulde-Ferrell-Larkin-Ovchinnikov state in heavy fermion superconductors, J. Phys. Soc. Jpn. **76**, 051005 (2007).
[7] G. B. Partridge, W. Li, R. I. Kamar, Y. A. Liao, and R. G. Hulet, Pairing and phase separation in a polarized Fermi gas, Science **311**, 503 (2006).
[8] M. M. Parish, S. K. Baur, E. J. Mueller, and D. A. Huse, Quasi-one-dimensional polarized fermi superfluids, Phys. Rev. Lett. **99**, 250403 (2007).
[9] C.-X. Liu, Unconventional superconductivity in bilayer transition metal dichalcogenides, Phys. Rev. Lett. **118**, 087001 (2017).
[10] D. Zhao, L. Debbeler, M. Kühne, S. Fecher, N. Gross, and J. Smet, Evidence of finite-momentum pairing in a centrosymmetric bilayer, Nat. Phys. **19**, 1599 (2023).
[11] P. Wan, O. Zheliuk, N. F. Q. Yuan, X. Peng, L. Zhang, M. Liang, U. Zeitler, S. Wiedmann, N. E. Hussey, T. T. M. Palstra, and J. Ye, Orbital Fulde-Ferrell-Larkin-Ovchinnikov state in an Ising superconductor, Nature (London) **619**, 46 (2023).
[12] M. Croitoru and A. Buzdin, In search of unambiguous evidence of the Fulde-Ferrell-Larkin-Ovchinnikov state in quasi-low dimensional superconductors, Condens. Matter **2**, 30 (2017).
[13] J. Schirmer, J. K. Jain, and C. X. Liu, Topological superconductivity induced by spin-orbit coupling, perpendicular magnetic field, and superlattice potential, Phys. Rev. B **109**, 134518 (2024).
[14] H. Watanabe, A proof of the Bloch theorem for lattice models, J. Stat. Phys. **177**, 717 (2019).
[15] P. F. Bagwell, Critical current of a one-dimensional superconductor, Phys. Rev. B **49**, 6841 (1994).
[16] G.-W. Qiu and Y. Zhou, Inhomogeneous superconducting states in two weakly linked superconducting ultrathin films, Phys. Rev. B **105**, L100506 (2022).
[17] V. L. Pokrovsky and A. L. Talapov, Ground state, spectrum, and phase diagram of two-dimensional incommensurate crystals, Phys. Rev. Lett. **42**, 65 (1979).
[18] K. Yang, K. Moon, L. Zheng, A. H. MacDonald, S. M. Girvin, D. Yoshioka, and S.-C. Zhang, Quantum ferromagnetism and phase transitions in double-layer quantum Hall systems, Phys. Rev. Lett. **72**, 732 (1994).
[19] K. Yang, K. Moon, L. Belkhir, H. Mori, S. M. Girvin, A. H. MacDonald, L. Zheng, and D. Yoshioka, Spontaneous interlayer coherence in double-layer quantum Hall systems: Symmetry-breaking interactions, in-plane fields, and phase solitons, Phys. Rev. B **54**, 11644 (1996).
[20] M. Stone and S.-B. Chung, Fusion rules and vortices in $p_x + ip_y$ superconductors, Phys. Rev. B **73**, 014505 (2006).
[21] M. Oshikawa, Y. B. Kim, K. Shtengel, C. Nayak, and S. Tewari, Topological degeneracy of non-Abelian states for dummies, Ann. Phys. (NY) **322**, 1477 (2007).
[22] C. Nayak, S. H. Simon, A. Stern, M. Freedman, and S. Das Sarma, Non-Abelian anyons and topological quantum computation, Rev. Mod. Phys. **80**, 1083 (2008).
[23] J. D. Sau, R. M. Lutchyn, S. Tewari, and S. Das Sarma, Generic new platform for topological quantum computation using semiconductor heterostructures, Phys. Rev. Lett. **104**, 040502 (2010).
[24] T. D. Stanescu, J. D. Sau, R. M. Lutchyn, and S. Das Sarma, Proximity effect at the superconductor-topological insulator interface, Phys. Rev. B **81**, 241310(R) (2010).
[25] J. Alicea, New directions in the pursuit of Majorana fermions in solid state systems, Rep. Prog. Phys. **75**, 076501 (2012).
[26] H.-H. Hung, P. Ghaemi, T. L. Hughes, and M. J. Gilbert, Vortex lattices in the superconducting phases of doped topological insulators and heterostructures, Phys. Rev. B **87**, 035401 (2013).
[27] C. W. J. Beenakker, Search for Majorana fermions in superconductors, Annu. Rev. Condens. Matter Phys. **4**, 113 (2013).
[28] J. Zhou, Y.-J. Wu, R.-W. Li, J. He, and S.-P. Kou, Hierarchical topological superconductor—A Majorana vortex lattice model, Europhys. Lett. **102**, 47005 (2013).
[29] R. R. Biswas, Majorana fermions in vortex lattices, Phys. Rev. Lett. **111**, 136401 (2013).
[30] S. D. Sarma, M. Freedman, and C. Nayak, Majorana zero modes and topological quantum computation, npj Quantum Inf, **1**, 15001 (2015).
[31] T. Liu and M. Franz, Electronic structure of topological superconductors in the presence of a vortex lattice, Phys. Rev. B **92**, 134519 (2015).
[32] J. M. Murray and O. Vafek, Majorana bands, Berry curvature, and thermal Hall conductivity in the vortex state of a chiral p-wave superconductor, Phys. Rev. B **92**, 134520 (2015).
[33] E. D. B. Smith, K. Tanaka, and Y. Nagai, Manifestation of chirality in the vortex lattice in a two-dimensional topological superconductor, Phys. Rev. B **94**, 064515 (2016).
[34] https://github.com/uddaloknag/Bilayer-SC-Data-PRB.